

On the relationship between satellite-retrieved surface temperature fronts and chlorophyll *a* in the western South Atlantic

Martin Saraceno and Christine Provost

Laboratoire d'Océanographie Dynamique et de Climatologie, UMR 7617, CNRS, IRD-UPMC-MNHN, Institut Pierre Simon Laplace, Université Pierre et Marie Curie, Paris, France

Alberto R. Piola

Departamento de Oceanografía, Servicio de Hidrografía Naval, Buenos Aires, Argentina

Departamento de Ciencias de la Atmósfera y los Océanos, Facultad de Ciencias Exactas y Naturales, Universidad de Buenos Aires, Buenos Aires, Argentina

Received 1 October 2004; revised 4 June 2005; accepted 29 August 2005; published 18 November 2005.

[1] The time-space distribution of chlorophyll *a* in the southwestern Atlantic is examined using 6 years (1998–2003) of sea surface color images from Sea-viewing Wide Field of View Sensor (SeaWiFS). Chlorophyll *a* (chl *a*) distribution is confronted with sea surface temperature (SST) fronts retrieved from satellite imagery. Histogram analysis of the color, SST, and SST gradient data sets provides a simple procedure for pixel classification from which eight biophysical regions in the SWA are identified, including three new regions with regard to Longhurst (1998) work: Patagonian Shelf Break (PSB), Brazil Current Overshoot, and Zapiola Rise region. In the PSB region, coastal-trapped waves are suggested as a possible mechanism leading to the intraseasonal frequencies observed in SST and chl *a*. Mesoscale activity associated with the Brazil Current Front and, in particular, eddies drifting southward is probably responsible for the high chl *a* values observed throughout the Brazil Current Overshoot region. The Zapiola Rise is characterized by a local minimum in SST gradient magnitudes and shows chl *a* maximum values in February, 3 months later than the austral spring bloom of the surroundings. Significant interannual variability is present in the color imagery. In the PSB, springs and summers with high chl *a* concentrations seem associated with stronger local northerly wind speed, and possible mechanisms are discussed. Finally, the Brazil-Malvinas front is detected using both SST gradient and SeaWiFS images. The time-averaged position of the front at 54.2°W is estimated at 38.9°S and its alongshore migration of about 300 km.

Citation: Saraceno, M., C. Provost, and A. R. Piola (2005), On the relationship between satellite-retrieved surface temperature fronts and chlorophyll *a* in the western South Atlantic, *J. Geophys. Res.*, 110, C11016, doi:10.1029/2004JC002736.

1. Introduction

1.1. Sea Surface Temperature Fronts and Color Satellite Images

[2] Since September 1997 the ocean color sensor Sea-viewing Wide Field of View Sensor (SeaWiFS) has been providing an outstanding data set for a wide range of studies, involving large-scale oceanic biological productivity. Chlorophyll abundance is associated with fronts, eddies and regions of upwelling. Thus SeaWiFS records are useful for studying physical processes in the ocean [e.g., *McGillicuddy et al.*, 1998; *Fratantoni and Glickson*, 2002].

[3] In this article, we use chlorophyll *a* (chl *a*) as a water mass tracer. Although chl *a* is a nonconservative quantity, near surface chl *a* concentrations are more or less homogeneous within a given water body (a given current or an eddy)

and changes in chl *a* concentration can be used to delineate boundaries of eddies or currents, i.e., oceanic fronts [*Quartly and Srokosz*, 2003]. Fronts are locally marked by high levels of chlorophyll *a* when the mixing between two adjacent water masses provides the optimal conditions for growth (nutrients, light, warmth and enhanced mixing and upwelling) that neither water masses contain alone [*Quartly and Srokosz*, 2003]. The objective of the present paper is to compare chl *a* distribution with SST and SST gradient fields in the southwestern Atlantic (SWA) Ocean using satellite data. Highest values in SST gradient fields are used as a proxy for the surface thermal fronts. The SWA stands out as one of the regions of the world ocean with highest concentration and most complex distribution of chl *a*. The high concentration of chl *a* is associated with high primary productivity, and a major fishery [*Food and Agricultural Organization*, 1972]. Improving our knowledge on the spatial distribution of chl *a* and on the relationship between chl *a* and SST fronts is crucial for living

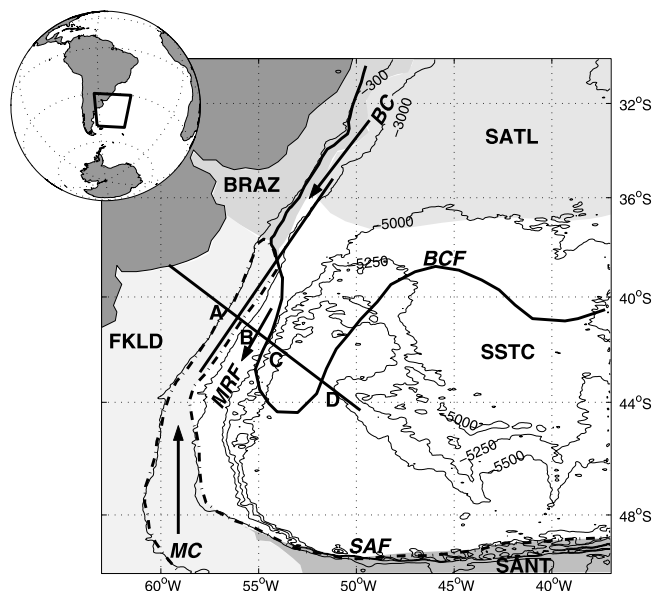


Figure 1. Schematic diagram of major fronts and currents in the western South Atlantic. The collision between the Malvinas Current (MC) and Brazil Current (BC) occurs near 38°S. After collision with the BC, the main flow of the MC describes a sharp cyclonic loop, forming the Malvinas Return Flow (MRF). The mean positions of the Brazil Current Front (BCF, solid line) and the Subantarctic Front (SAF, dash-dotted line) are from Saraceno *et al.* [2004]. The different shaded regions are from Longhurst's [1998] biophysical provinces in the southwestern Atlantic (SWA): South Atlantic Gyral Province (SATL), Brazil Current Coastal Province (BRAZ), Southwest Atlantic Shelves Province (FKLD), South Subtropical Convergence Province (SSTC), and Subantarctic Water Ring Province (SANT). Isobaths at 300, 3000, 5000, 5250, and 5500 m are represented [from Smith and Sandwell, 1994]. The Zapiola Rise feature is observed at 45°W, 45°S. The along- and cross-shelf sections (solid black segments) used to plot the Hovmöller diagrams in Figures 5 and 13 are also indicated. Letters indicate the intersection between the cross-shelf section and the shelf break front (A), the Malvinas Return Front (B), and the BCF (C and D). These points correspond to local maxima in SST gradient and chl *a* along the section (Figure 5).

resources management. High fishery activity is present in the frontal regions [e.g., Bisbal, 1995]. In particular, the Patagonian shelf break has been shown to be an economic and ecologically important region where the presence of species such as anchovy (*E. anchoita*) or hake (*M. hubbsi*) during 5–6 months of the year are associated with the Patagonian shelf break front [Acha *et al.*, 2004]. The large primary productivity is also likely to affect the regional balance of CO₂ on the Patagonian shelf [Bianchi *et al.*, 2005].

1.2. Southwestern Atlantic Ocean

1.2.1. Physical Characteristics

[4] The SWA Ocean is characterized by the Brazil/Malvinas Confluence region. The distribution of the chl *a*

concentration in the Confluence region reflects the complex ocean circulation patterns of the SWA. The Confluence is formed by the collision between the Malvinas Current (MC) and the Brazil Current (BC) approximately at 38°S (Figure 1) and makes the region one of the most energetic of the world ocean [Gordon, 1981; Chelton *et al.*, 1990]. The MC is part of the northern branch of the Antarctic Circumpolar Current [Piola and Gordon, 1989] that carries the cold and relatively fresh subantarctic water equatorward along the western edge of the Argentine Basin. The BC flows poleward along the continental margin of South America as part of the western boundary current of the South Atlantic subtropical gyre. After its collision with the MC, the BC flows southward and, at about 44°S, returns to the NE. This path is commonly referred to as the overshoot of the Brazil Current [e.g., Peterson and Stramma, 1991].

[5] Two major oceanic fronts are present in the SWA: the Subantarctic Front (SAF) and the Brazil Current Front (BCF). The former is the northern boundary of subantarctic water and the latter is the southern limit of South Atlantic Central Water. Bottom topography plays an important role controlling the location of the SAF. The Shelf Break Front and the Malvinas Return Front are part of the SAF and correspond respectively to the western and eastern boundaries of the MC: their position is established by the sharp bottom slope at the shelf edge following approximately the 300 and 3000 m depths, respectively [Saraceno *et al.*, 2004] (Figure 1). Bathymetry is also responsible for the low SST gradient magnitude observed above the Zapiola Rise [Saraceno *et al.*, 2004]. The position where the Brazil and Malvinas currents collide is not controlled by bottom topography and the variability of the position of the resulting front is a subject of controversial results. Using AVHRR data from 1981 to 1987, Olson *et al.* [1988] estimate that the separation points of the BCF and SAF from the 1000 m isobath occurs around $35.8 \pm 1.1^\circ\text{S}$ and $38.6 \pm 0.9^\circ\text{S}$ respectively. Using a combination of altimeter and thermocline depth data, Goni and Wainer [2001] find that in the period 1993–1998 the separation of the BCF from the 1000 m isobath depth occurs, on average, at $38.5 \pm 0.8^\circ\text{S}$. Computing SST frontal probabilities from nine years of AVHRR data, Saraceno *et al.* [2004] find evidence that the SAF and BCF merge into a single surface front in the collision region. In the lee of the collision region (east of 53.5°W) the two fronts diverge (Figure 1) [Gordon and Greengrove, 1986; Roden, 1986]. In the collision region, the single front pivots seasonally, around a fixed point located at 39.5°S, 53.5°W [Saraceno *et al.*, 2004]. In winter the front is orientated N-S along 53.5°W and in summer it shifts to a NW-SE direction. Because this front separates water masses with distinct thermohaline and nutrient characteristics, the frontal displacements produce a strong impact on the distribution of biota [e.g., Brandini *et al.*, 2000]. Thus the Brazil/Malvinas frontal motion should be detectable in satellite color images, possibly providing independent evidence of the frontal displacements.

1.2.2. Biophysical Regions

[6] Chl *a* concentration can be used to identify biogeographical regions in the ocean. Longhurst [1998] (hereinafter referred to as L98) discusses concisely the large-scale chl *a* distributions and the major forcing responsible for the chl

a concentration in each biogeochemical province that he defined. L98 determines provinces considering several databases: chlorophyll fields obtained from the coastal zone color scanner (CZCS) sensor, global climatologies of mixed layer depth, Brunt-Väisälä frequency, Rossby internal radius of deformation, photic depth and surface nutrient concentrations. L98 defines five Provinces in the SWA (Figure 1): The Southwest Atlantic Shelves Province (FKLD) is limited by the 2000 m isobath to the east. Tidal forcing on the shelf is supposed to be the major forcing of the spring and summer bloom concentrations of chl *a* (L98). Dynamic eddying is proposed as the main mechanism causing the high concentration values through the shelf break, where a linear chlorophyll feature is observed in a high percentage of days, especially in summer (L98). The Brazil Current Coastal Province (BRAZ) is limited by the 2000 m isobath to the east and by the confluence between the Brazil and Malvinas currents to the south. A sharp turbidity front marks the limit of tidal stirring near the mouth of the Plata river [Framiñan and Brown, 1996; L98]. The South Atlantic Gyral Province (SATL) comprises the South Atlantic anticyclonic circulation, where surface chlorophyll values are low throughout the year over most of the area. The portion of the Subantarctic Water Ring Province (SANT) comprised in the SWA has an oligotrophic regime. The South Subtropical Convergence (SSTC) Province presents a strong biological enrichment during all seasons (L98).

1.3. Outline

[7] After presenting the data and methods in section 2, eight biophysical regions are identified based on histogram analysis of SST, SST gradient and chl *a* mean distributions (section 3). The chl *a* time-space variability and its relationship with thermal fronts in the Patagonian Shelf break (PSB), Brazil Current overshoot and Zapiola Rise regions are examined in section 4. The Brazil-Malvinas collision front as seen with SST gradient and SeaWiFS images is also described in section 4. Summary and discussion of the main results, including further analysis of the chl *a* interannual variability, follows in section 5.

2. Data and Methods

[8] We use six years (January 1998 to December 2003) of SeaWiFS images and four different sources of satellite derived SST based on Advanced Very High Resolution Radiometer (AVHRR) or microwave measurements. The AVHRR data used cover different time periods and have different spatial resolution and characteristics according to the processes applied to produce the SST and the cloud masking. The three AVHRR data are (1) data received at a local station in Argentina and processed at the Rosenstiel School of Marine and Atmospheric Science, University of Miami (RSMAS); (2) version 4.1 produced by the Jet Propulsion Laboratory (JPL), and (3) the optimal interpolated data set from Reynolds and Smith [1994]. Microwave measurements are from the Advanced Microwave Scanning Radiometer for Eos (AMSR-E) [Wentz and Meissner, 2004]. Detailed description of each database follows below.

[9] Phytoplankton pigment concentrations are obtained from 8 day average composite SeaWiFS products of level 3 binned data, generated by the NASA Goddard Space Flight

Center (GSFC) Distributed Active Archive Center (DAAC) with reprocessing 4 [McClain *et al.*, 1998]. The bins correspond to approximately 9×9 km grid cells on a global grid.

[10] The RSMAS data set cover the period from January 1986 to December 1995. It is composed of 697 images 5 day composite with approximately 4×4 km resolution. Cloud detection (G. Podestá, personal communication, 2004) was done applying a median filter with a window size of 5×5 pixels through the individual images (corresponding to a single pass). All pixels over water with estimated temperatures below 3°C were flagged as clouds. Whenever a pixel in the box differed by more than 2°C from the median of the box, it was also flagged as cloud contaminated. Compositing was made conserving the warmest temperature observed during the 5 day period for each pixel. This composite reduces the effect of cloud coverage and the likelihood of negative biases due to cloud contamination [Podestá *et al.*, 1991]. A seasonal analysis of the cloud coverage in the SWA using the same data set was carried out by Saraceno *et al.* [2004]. It is shown that the difference between summer and winter cloud cover is lower than 10%. Using NCEP (National Center of Environmental Prediction) and ECWMF (European Centre for Medium Weather Forecasting) reanalysis in the SWA, Escoffier and Provost [1998] find similar low seasonal variability in cloud cover. Thus we consider that the seasonal cloud cover variability does not affect the results.

[11] The RSMAS SST and color time series are not concomitant. We consider the 8 day composite with 9×9 km of spatial resolution of version 4.1 of the AVHRR data from JPL to fill the gap. Version 4.1 assigns excessive cloud coverage in regions with strong thermal gradients [Vazquez *et al.*, 1998]. The front in the Brazil/Malvinas collision region is constantly covered by “clouds” in those images (not shown). Version 4.1 ends on July 2003. The latest version (5.1) which spans up-to-date and has a 4×4 km spatial resolution presents large regions with constant artificial cloud masking in the SWA (as confirmed by J. Vazquez, personal communication, 2004). Thus we use the 4.1 version to analyze the SST and SST gradient in those regions of the SWA where gradient values are not too high (i.e., in the shelf and shelf break region).

[12] Because of the lower spatial resolution (one by one degree), Reynolds data are not adequate to compare the frontal thermal structures (SST gradient) with color images. However, they are useful when SST time series are considered.

[13] Finally, to compare color and SST distributions at the confluence of the Brazil/Malvinas front, AMSR-E [Wentz and Meissner, 2004] data are used. AMSR-E data are available since June 2002 and are cloud free. Their spatial resolution is about 25 km.

[14] For each SST image of the RSMAS, 4.1 JPL and AMSR-E data set, an SST gradient image is produced conserving the respective spatial resolution. SST gradient magnitude fields were produced using a Prewitt operator [Russ, 2002] using a window of about 30×30 km (corresponding to 7×7 pixels for the RSMAS, 3×3 pixels for the 4.1 JPL and 1×1 pixel for the AMSR-E data set). This box size retains the large and mesoscale frontal features with an acceptable amount of noise.

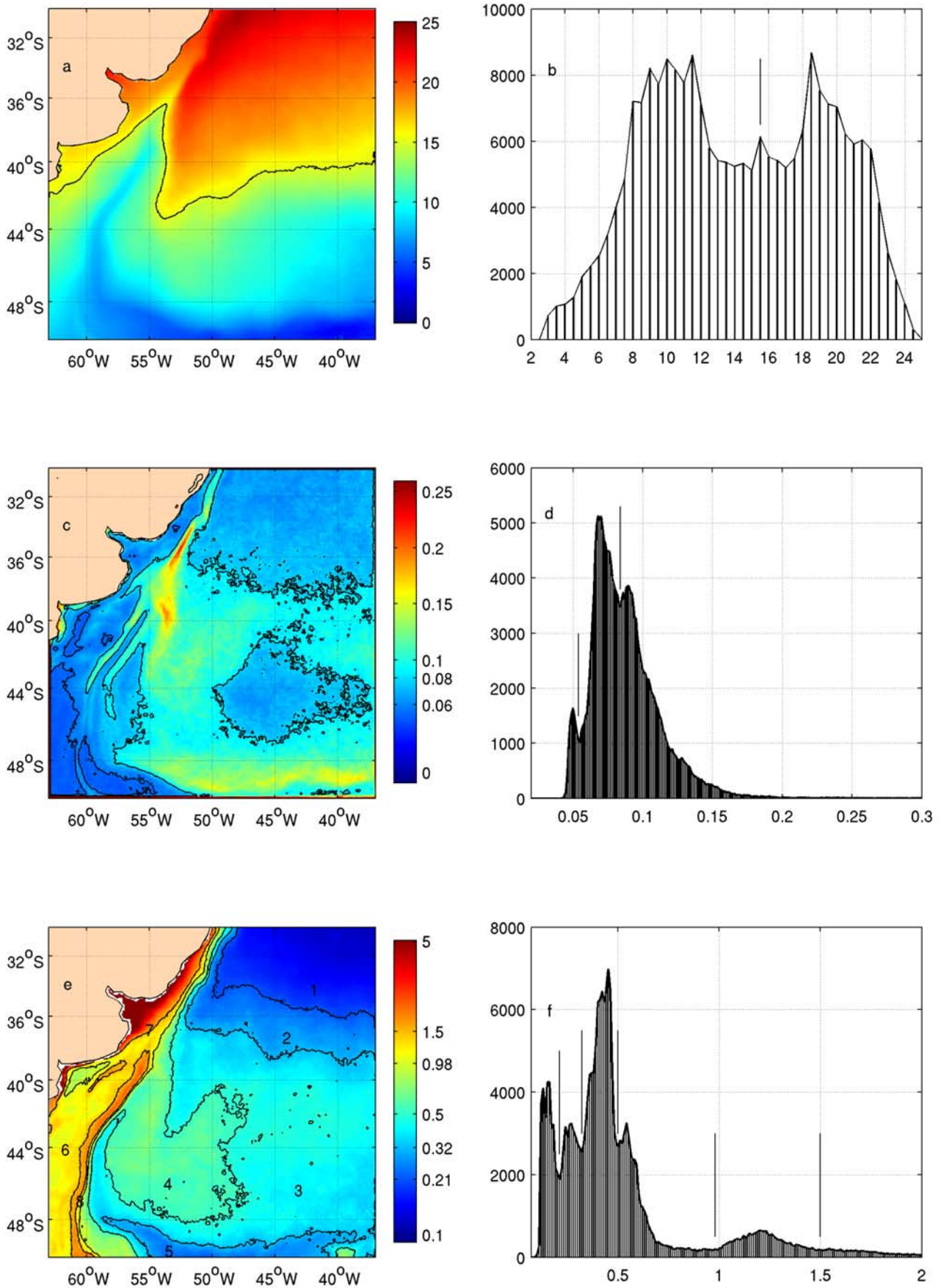


Figure 2

Table 1. Classification of SST, SST Gradient, and chl *a* According to the Respective Histograms for the Mean Images

	Thresholds
SST, °C	16
Grad SST, °C/km	0.06, 0.08
Chl <i>a</i> mg/m ³	0.21, 0.32, 0.5, 0.88, 1.5

[15] In order to calculate spectra of SST time series extracted at certain locations (section 4.1), cloudy pixels in the time series are filled using a cubic spline interpolation. Cloudy pixels in the time series represent less than 8% of the record length. Spectra, confidence limits (CL) and significant peaks of the time series are then calculated using the singular spectrum analysis multitaper method toolkit [Ghil *et al.*, 2002]. Two data tapers are used and significant peaks have been estimated with the hypothesis of a harmonic process drawn back in a background red noise.

[16] To investigate possible forcing mechanisms for the variability observed in chl *a*, surface wind data were analyzed. We consider satellite scatterometer data from QuikSCAT between January 2000 and December 2003 (<http://www.ifremer.fr/cersat/fr/data/overview/gridded/mwfsqcat.htm>). The wind satellite data are daily and have a spatial resolution of 0.5°.

3. Identification of Regions

[17] The 10 year mean of SST and SST gradient fields from RSMAS and the 6 year mean of chl *a* fields together with their respective histograms (Figure 2) are used to identify biophysical regions in the SWA. Histogram analysis is largely used in image analysis for objective pixel classification [e.g., Russ, 2002]. Histograms of mean images (Figures 2b, 2d, and 2f) show that chl *a* and SST gradient magnitude have a multimodal structure, while SST can be considered as bimodal. The local minima in the histograms determine the thresholds used to classify pixels in the mean images (Table 1).

[18] The 10 year RSMAS SST mean (Figure 2a) encompasses values from 2°C in the south to 25°C in the north. Isotherms present strong curvatures associated with the convoluted paths of the Malvinas and Brazil currents (see Figure 1). The corresponding histogram separates SST in relatively warm (>16°C) and cold (<16°C) surface waters.

[19] The 10 year mean of RSMAS SST gradient (Figure 2c) is an average representation of the fronts in the SWA [Saraceno *et al.*, 2004]. The image defines precise limits of water masses in the upper ocean. It also contains useful information on the mesoscale activity of the SWA: for example, the BCF in the overshoot region is quite diffuse and presents relatively low SST gradients because of the high spatial variability of water mass structure. The mean positions of the SAF and BCF (illustrated in Figure 1) correspond to the SST gradient maxima shown in Figure 2c.

Centered at 45°S, 45°W, the Zapiola Rise is a region with low SST gradients. Thresholds determined from the SST gradient histogram define three distinct ranges (Table 1). Values over the Zapiola Rise range between 0.06 and 0.08°C/km. The BCF, the Shelf Break Front and the Malvinas Return Front north of 45°S and the SAF south of 47°S present values higher than 0.08°C/km. Values lower than 0.06°C/km are found in small regions, mostly located in the southwest of the domain.

[20] The 6 years mean color distribution from SeaWiFS shows a wide range of chlorophyll values in the SWA: from oligotrophic regions to regions that exhibits concentrations higher than 5 mg/m³. The histogram presents five local minima or thresholds (Table 1) that classify pixels into six different ranges of values that establish eight major areas in the SWA (Figure 2e).

[21] The superposition of the regions derived from the threshold classification shows that most of the boundaries defined by the SST gradient regions are common with the boundaries of the regions defined by chl *a* (Figure 3a). Eight biophysical regions (Figure 3b) present one or more variables that identify each region uniquely (Table 2). Chl *a* defines main regions and the SST threshold separates those that have common chl *a* concentrations: PSB from BRAZ and SATL from SANT. In addition, the 0.08°C/km gradient threshold is critical to identify the Zapiola Rise. Three of these regions coincide with the L98 classification into Provinces (SANT, BRAZ and SATL) and three new regions appear, which subdivide the SSTC and FKLD Provinces into subregions (Figure 3 and Table 2). The SSTC Province contains the Zapiola Rise and the Overshoot regions; and the FKLD Province contains the PSB region.

[22] The regions identified in this section arise from the mean fields, thus variability on interannual or seasonal timescale is not considered. The spatiotemporal variability of the chl *a* and its relationship with thermal fronts is discussed in the next section; the evolution of the boundaries of biophysical regions with time deserves further analysis and will be the subject of a future work.

4. Specific Features

[23] In the previous section, three new regions with regard to L98 Provinces were identified. Below we describe the relationship between SST fronts and chl *a* on these regions and at the Brazil-Malvinas collision front. Time variations are described considering monthly climatologies of SST, SST gradient and chl *a* fields (Figure 4) and two space-time sections (across shelf in Figure 5 and along shelf in Figure 13).

4.1. Patagonian Shelf Break

[24] The PSB region is characterized by one of the longest (~1000 km) blooms of chl *a* of the world ocean. The bloom is clearly visible in February from 38°S to the

Figure 2. (a) Ten years (1986–1995) mean of SST (°C), (c) 10 years (1986–1995) mean of SST gradient (°C/km), and (e) 6 years (1998–2003) mean of chl *a* (mg/m³). Histograms in units of (b) number of pixels (y axis) and °C, (d) °C/km, and (f) mg/m³. In Figures 2a, 2c, and 2e, thin black contour lines correspond to the local minima indicated with a vertical line in the corresponding histograms (see Table 1); numbers on Figure 2e indicate the eight major areas defined by the chl *a* histogram.

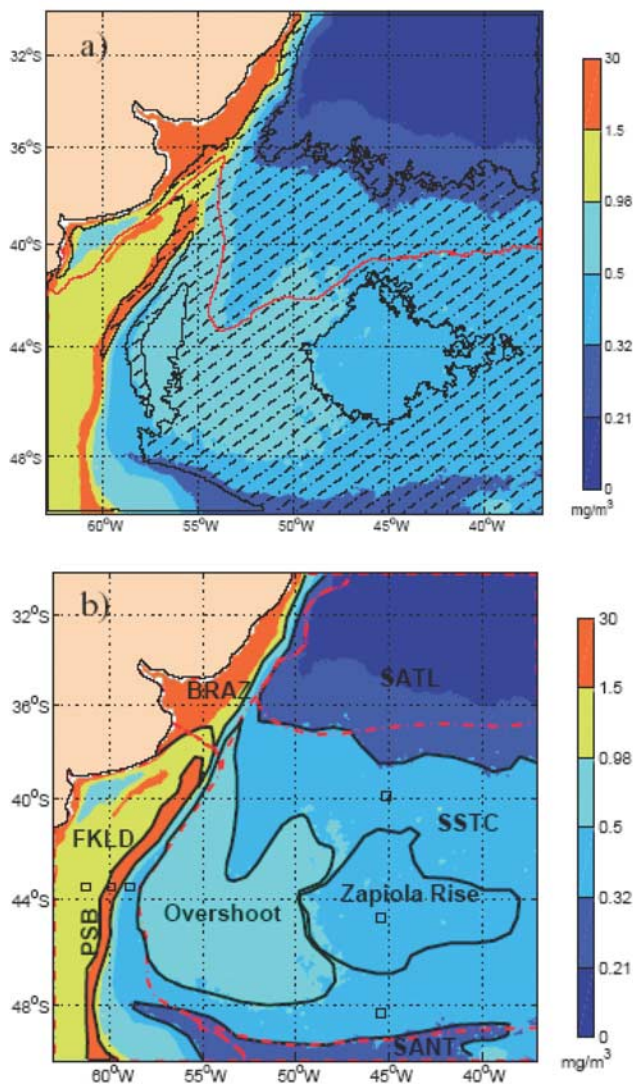


Figure 3. (a) Six ranges of chl *a* magnitudes based on the respective histogram, represented by background colors. The hatched region indicates areas with SST gradients higher than $0.08^{\circ}\text{C}/\text{km}$. The solid red line is the threshold deduced from the SST field. (b) Information from the three mean fields (SST, chl *a*, and SST gradient) synthesized and compared to L98 mean definition of Provinces in the SWA Ocean, with background colors as in Figure 3a. Regions obtained from histograms are indicated with solid black lines, and L98 provinces (BRAZ, SSTC, SANT, SATL, FKLD) are indicated with dashed red lines. Small boxes north, south, and within the Zapiola Rise Region and east, west, and within the Patagonian Shelf Break (PSB) indicate the position where time series are extracted (Figures 6 and 12).

south of the domain along the western branch of the SAF (Figure 4). The high SST gradient magnitudes associated to this bloom ($>0.08^{\circ}\text{C}/\text{km}$ north of 44°S , Figure 3) correspond to the Patagonian shelf break front [Legeckis and Gordon, 1982; Acha et al., 2004; Saraceno et al., 2004] that separates the Subantarctic shelf waters from the colder and more saline waters of the MC [Martos and Piccolo, 1988].

The PSB region is clearly visible in the cross-shelf section (Figure 5) associated with the local maxima of chl *a* and SST gradient at 56.6°W . Both local maxima correspond in time and space and are located over the topographic shelf break, emphasizing the strong topographic control (Figure 5).

[25] Over the shelf and in the core of the MC (west and east of the PSB region respectively) the time evolution of the chl *a* is quite different (Figure 6). Chl *a* concentrations start increasing in September in the three time series. From August to April, the PSB region presents higher concentration with regard to surrounding waters. Values over the shelf and at the PSB reach their maximum in October ($\sim 3.5 \text{ mg}/\text{m}^3$) while values in the MC reach their maximum in September and decay to a mean value of $\sim 0.5 \text{ mg}/\text{m}^3$ during the rest of the year. Thus the presence of the shelf break front is responsible for the higher chl *a* values over the PSB region. Different processes associated with the shelf break front could induce a vertical circulation [Huthnance, 1995] that may enhance a higher transport of nutrients to the euphotic zone than over the Patagonian shelf or in the MC. To date, such a process in the PSB region has not been documented in the literature, while several propositions were made. Erickson et al. [2003] suggested that iron can be transported from the South American continent by westerly winds and fertilize the adjacent South Atlantic Ocean. This kind of fertilization affects large areas and is therefore unlikely to explain by itself the higher productivity over the narrow PSB region. L98 proposed that enhanced topographically driven mesoscale activity (i.e., eddies) could also play a role in generating the higher values observed over the PSB region. However, the higher percentage of eddies that creates at the B/M Collision region drift southeastward rather than westward [Lentini et al., 2002] and there is no evidence of eddies reaching the PSB region. Acha et al. [2004] additionally suggested that internal waves, coupled with episodic wind stress, are a possible mechanism to enhance the supply of the nutrient-rich MC to the euphotic zone. Finally, Podestá [1990] suggested that the interleaving of water masses at the front could enhance vertical stability, retaining phytoplankton cells in the euphotic zone.

4.1.1. Seasonal and Intraseasonal Variability

[26] Power spectral density of SST and chl *a* time series extracted in a box of one by one degree in the northern part of the PSB region shows significant peaks centered at the annual and intraseasonal frequencies (Figure 7). The annual peak is a common factor for the whole region, and has already been described both for the SST [e.g., Podestá et al., 1991; Provost et al., 1992] and for the chl *a* [e.g., L98;

Table 2. Southwest Atlantic Regional Characteristics

Region	L98 Province	chl <i>a</i> , mg/m^3	SST $^{\circ}\text{C}$	SST Gradient, $^{\circ}\text{C}/\text{km}$
SATL	SATL	<0.32	>16	<0.08
SSTC	SSTC	$0.32-0.5$	-	>0.08
Overshoot	SSTC	$0.5-0.98$	<16	>0.08
Zapiola Rise	SSTC	$0.32-0.5$	<16	<0.08
FKLD	FKLD	$0.98-1.5$	<16	<0.08
PSB	FKLD	>1.5	<16	>0.08 (north of 44°S)
BRAZ	BRAZ	>1.5	>16	<0.08
SANT	SANT	$0.21-0.32$	<16	>0.08

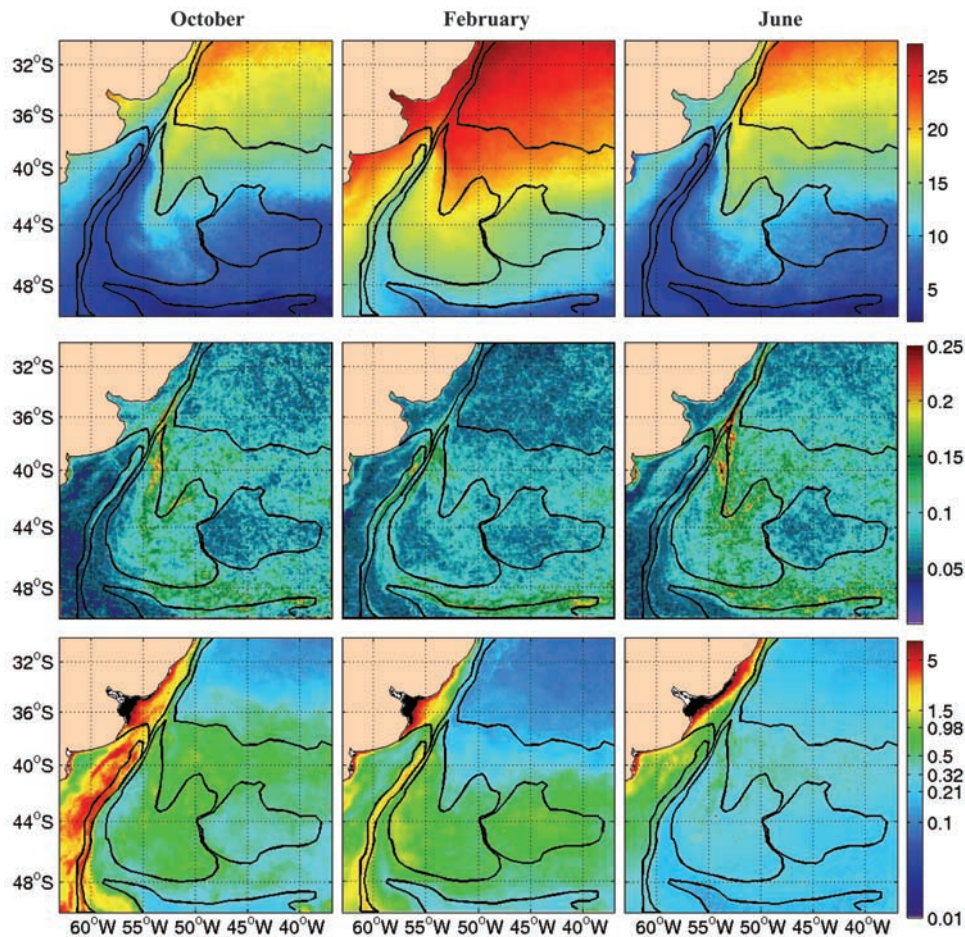


Figure 4. October, February, and June monthly climatologies of (top) SST ($^{\circ}\text{C}$), (middle) SST gradient ($^{\circ}\text{C}/\text{km}$), and (bottom) chl- a (mg/m^3). Black lines are limits of biophysical regions as defined in Figure 3b.

Garcia et al., 2004]. On the other hand, similar intra-seasonal peaks than those observed in Figure 7 are present along the PSB region (and not in adjacent regions, not shown) for the SST and chl a time series, suggesting that a process linked to the shelf break is responsible for the observed variability. We suggest that continental trapped waves (CTWs) could be the forcing mechanism. CTWs were already proposed to be present in the Patagonian shelf break by *Vivier et al.* [2001] to explain the 70 day fluctuations observed in the Malvinas Current transport and in SLA at 40°S [*Vivier and Provost*, 1999]. On the other hand, SSTs could be related to CTWs: along the coast of northern Chile, *Hormazabal et al.* [2001] show that SSTs are strongly modulated by CTWs. Thus we suggest that CTWs could be the forcing mechanism of the intraseasonal variability observed in the SST and color satellite data in the PSB region. This hypothesis supports the suggestion of internal waves made by *Acha et al.* [2004] to explain the higher values of chl a over the PSB. Further analyses are necessary to confirm the CTWs hypothesis or find other mechanisms to explain the intraseasonal variability observed and its origin. For instances, local wind do not seem to be related to CTWs: meridional and zonal components of the local wind do not show significant intraseasonal periodicities (not shown).

[27] The spectra of the SST time series also show a significant peak at the semiannual frequency (Figure 7b). Using shorter SST time series, *Provost et al.* [1992] showed that the ratio of the semiannual to the annual component in the PSB region represents a local maximum with reference to waters east and west of the shelf break. The semiannual frequency is associated with the semiannual wave present in the atmosphere at high southern latitudes [*Provost et al.*, 1992]. The semiannual peak is not significant in the chl a time series (Figure 7a).

4.1.2. Interannual Variability

[28] Chl a concentrations over the Patagonian shelf and shelf break present strong interannual variations (Figure 5). An overall trend of the spring concentrations to higher values is observed in the shelf and shelf break region (Figure 8). In particular, in the austral spring of 2003, chl a concentrations reach values twice higher than the concentrations observed during spring of previous years. In 1999, the spring bloom was present only during the first weeks of the season. To search the origin of the observed variability, we focus on the spring part of the time series of the time concomitant SST anomalies, meridional and zonal wind speed. SST anomalies and zonal wind speed do not exhibit any clear relationship with the chl a time series (Figure 9). On the other hand, the meridional wind speed

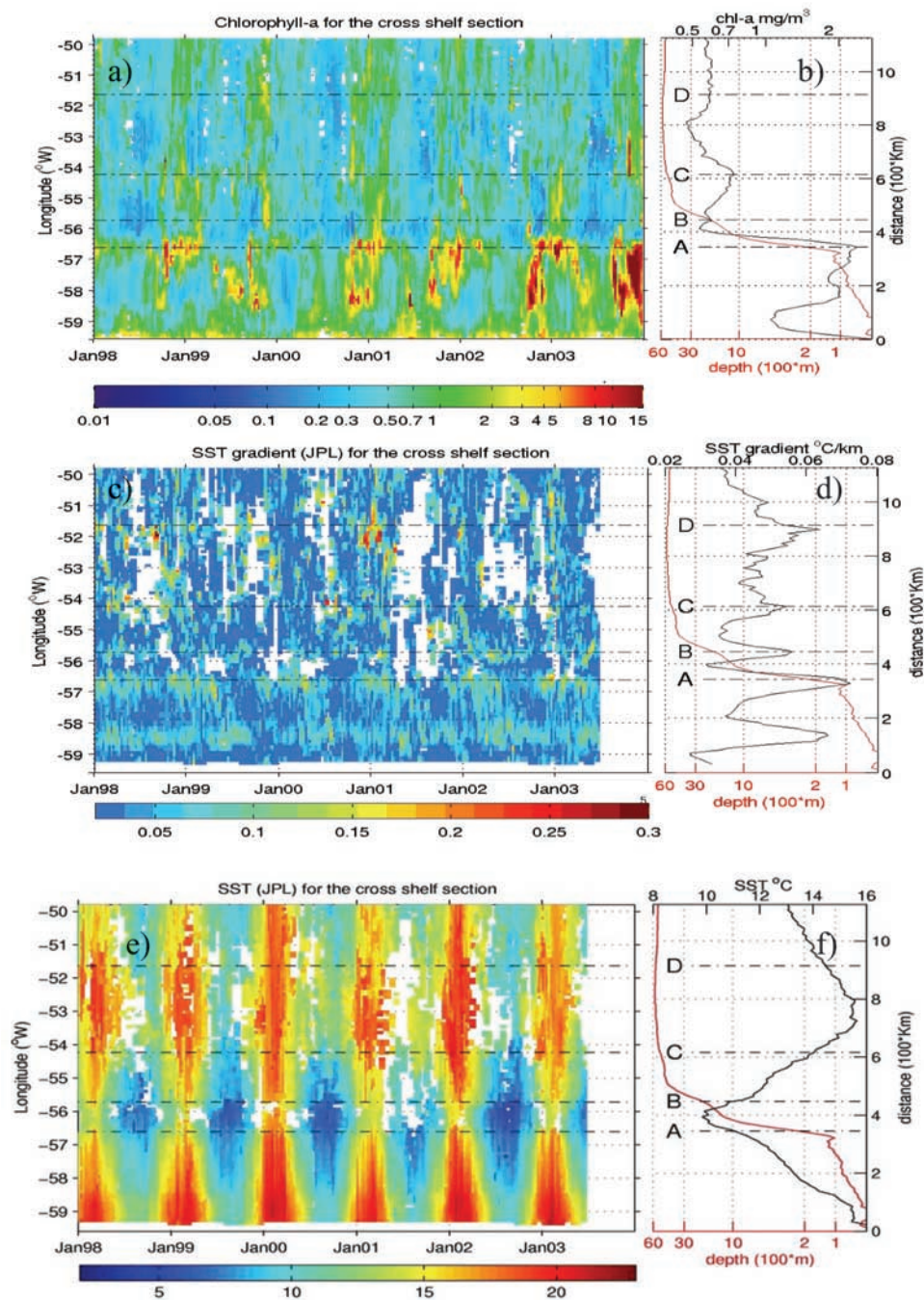


Figure 5. (a) Chl *a* (mg/m^3), (c) SST gradient ($^{\circ}\text{C}/\text{km}$), and (e) SST ($^{\circ}\text{C}$) versus time for the cross-shelf section. The position of the section is indicated in Figure 1. The bathymetry and the time average of the (b) chl *a*, (d) SST gradient, and (f) SST along the section is plotted to the right of the Hovmöller diagrams. Local chl *a* maxima are indicated with dash-dotted lines and reported on the SST and SST gradient sections. Chl *a* local maxima correspond to the intersection with the shelf break front (A), Malvinas Return front (B), and western (C) and eastern (D) branches of the BCF (see Figure 1). The local minima in three sections between points A and B correspond to the core of the Malvinas Current. White pixels on the Hovmöller diagrams indicate cloud-covered regions. Cloud coverage is higher in the overshoot region (between C and D) because the cloud-masking algorithm used by JPL assigns excessive masking to regions with high SST gradients [Vazquez *et al.*, 1998].

could explain part of the interannual variability: from September to December, northerly winds are higher in 2002 and 2003 than in 2000 and 2001 (Figure 10), corresponding respectively to the highest and lowest chl *a*

concentrations observed. Further, data suggest that the occurring date of the spring blooms is affected by the direction of the meridional wind speed (Figure 10): when southerly winds prevailed (i.e., late August and early

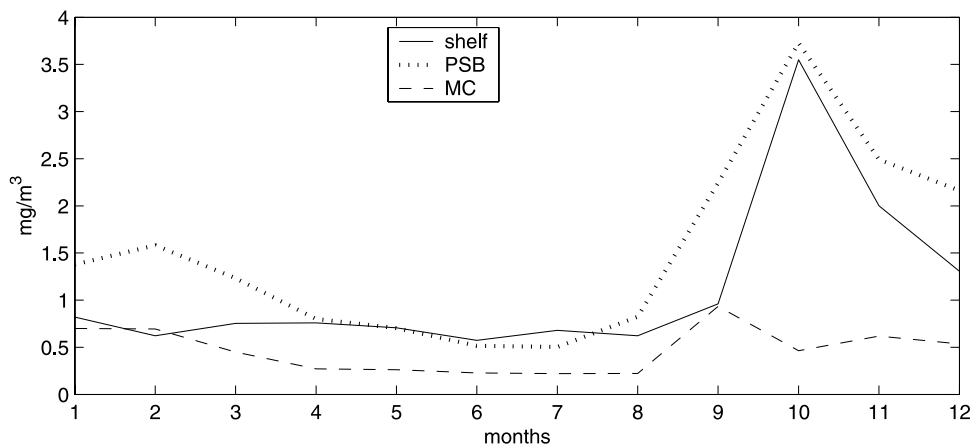


Figure 6. Chl *a* time series from the continental shelf (solid line), PSB (dotted line), and MC (dashed line). The location of the points where time series are extracted is indicated on Figure 3b. Each value in the time series is the monthly mean within a $\sim 30 \text{ km} \times 30 \text{ km}$ box.

September 2000 and 2002) the spring bloom occurred during the first days of October. Conversely, when northerly winds prevailed (i.e., late August and early September 2001 and 2003), the spring bloom took place during the first days of September.

[29] These observations further suggest that stronger northerly winds lead to higher chl *a* concentrations over the Patagonian shelf and shelf break regions. Northerly winds induce an eastward Ekman water mass transport in the southern hemisphere. The Ekman transport of the stratified shelf waters to the nutrient-rich waters of the Malvinas Current may result in the interleaving of the different water masses at the shelf break front that could enhance vertical stability, retaining phytoplankton cells in the euphotic zone [Podestá, 1990]. Brandini *et al.* [2000] have described similar water interleaving in the Brazil-Malvinas Confluence region as the mechanism responsible for the high chl *a* observed.

[30] In agreement with our results, Gregg *et al.* [2005] also observed a significant positive trend in chl *a* over the Patagonian shelf. They also found a negative trend in SST that was associated with increased upwelling. There is no conflict with our results (Figure 9) because the SST trend reported by Gregg *et al.* [2005] is based on all months of the year, while we just considered spring months. In fact, if all months are considered, we also find a negative trend in SST, that is associated with lower winter SSTs (not shown). Thus, to sustain the hypothesis of Gregg *et al.* [2005] for the Patagonian shelf chl *a* trend, a relation between higher winter upwelling and increased spring chl *a* is required. Understanding the relative role of winter upwelling, Ekman currents or other mechanisms that may lead to enhanced chl *a* concentrations, will require longer term satellite borne and in situ observations.

4.2. Brazil Current Overshoot

[31] In the overshoot region, chl *a* concentrations are higher than 1 mg/m^3 from September to March (see the climatologies for October and February in Figure 4). In austral winter, relatively high chl *a* concentrations are present only near the Brazil Current Front (BCF, see June in Figure 4). The BCF in the overshoot region has a U shape

and its southern part is centered approximately at 54°W , 44°S (Figures 1, 2, and 4). The western and eastern branches of the BCF are observed as two local maxima centered at 54.2°W and 51.6°W in the cross-shelf SST gradient and chl *a* sections (Figures 5d and 5b). Thus the concentration of chl *a* is enhanced along the BCF. The overshoot region is also characterized by warmer temperatures with reference to adjacent regions (Figure 5e). The advection of eddies coming from the BC are responsible for the higher temperatures. The mesoscale activity associated with the front and in particular eddies that drift southward are probably responsible for the high chl *a* values observed throughout the overshoot region. Chl *a* concentrations are known to be enhanced in high mesoscale activity regions [L98; Garçon *et al.*, 2001].

[32] Not all the overshoot region corresponds to SST gradients higher than 0.08°C/km : lower values are present in a region between the MRF and the BCF (between 42 and 47°S and 56 and 57°W , see Figures 3a and 4). In this particular region, chl *a* concentrations reach their maximum values three months later than in the surroundings (Figure 4). The region corresponds to low eddy kinetic energy values compared to the east of the overshoot region (Figure 11) indicating that fewer eddies are present. This observation is in agreement with the trajectories of eddies observed by Lentini *et al.* [2002]: eddies generated in the BCF drift southeastward rather than westward in the overshoot region. A lower eddy kinetic energy could explain lower chl *a* concentrations, but does not explain the 3 month lag of the chl *a* maximum.

4.3. Zapiola Rise

[33] The Zapiola Rise region stands out as a low SST gradient region throughout the year [Saraceno *et al.*, 2004]. The region extends over 1000 km in the zonal direction and 600 km in the meridional direction, and closely matches the location of the Zapiola Rise, centered at 45°S , 45°W (Figure 3).

[34] Chl *a* exhibits a local maximum in February and a minimum in October (Figure 4). From October to December (January to April), chl *a* concentrations over the rise are lower (higher), with reference to values north and south of

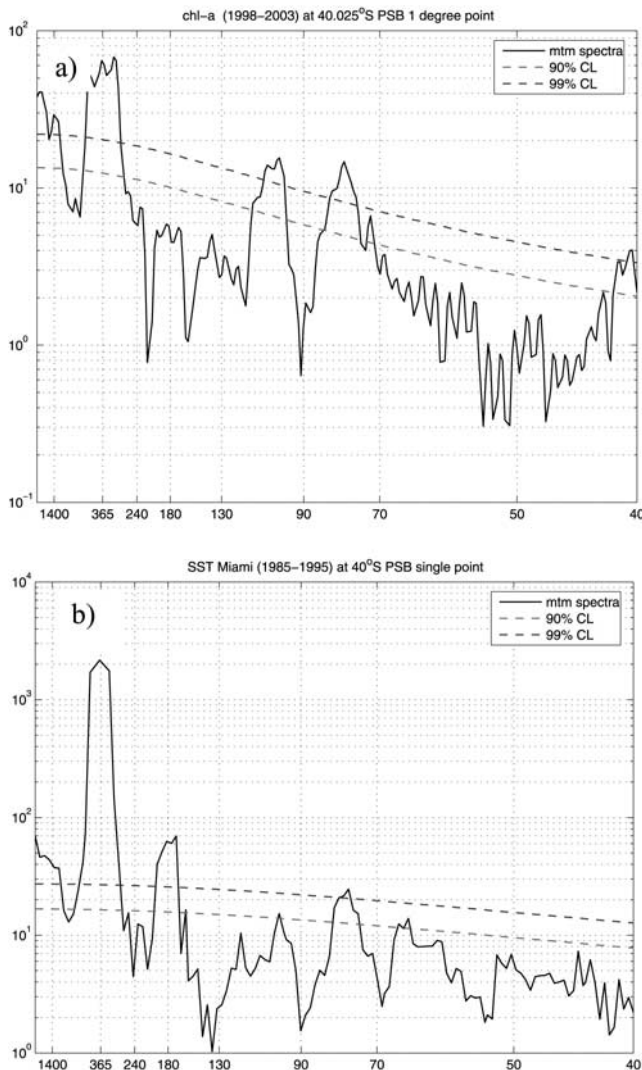


Figure 7. Power spectral density of (a) chl *a* and (b) RSMAS SST time series extracted in a 1° box side from the PSB region at 40.25°S , 56.73°W . The power spectral densities of the JPL SST and Reynolds SST time series in the same region present similar significant intraseasonal variability (not shown).

the region (Figure 12). From May to September, chl *a* concentrations are low (0.3 mg/m^3) and similar to the values observed further south (Figure 12). Maximum chl *a* concentrations north and south of the rise are reached in November (Figure 12; see Figure 3 for locations). *Dandonneau et al.* [2004] estimate the phase of the annual cycle in SeaWiFS chl *a* concentrations using 3 years (1998–2001) of monthly data averaged on a 0.5° longitude \times 0.5° latitude grid. Even with these lower spatial resolution and shorter time record length, the Zapiola Rise reaches its maximum amplitude in February, in agreement with our analysis. In addition, the Zapiola Rise is a region of relatively modest eddy kinetic energy, surrounded by areas of very high eddy energy levels associated with the SAF and BCF mesoscale activity (Figure 11). Thus sea surface height anomaly also suggests that the Zapiola Rise is distinct from the L98 SSTC Province.

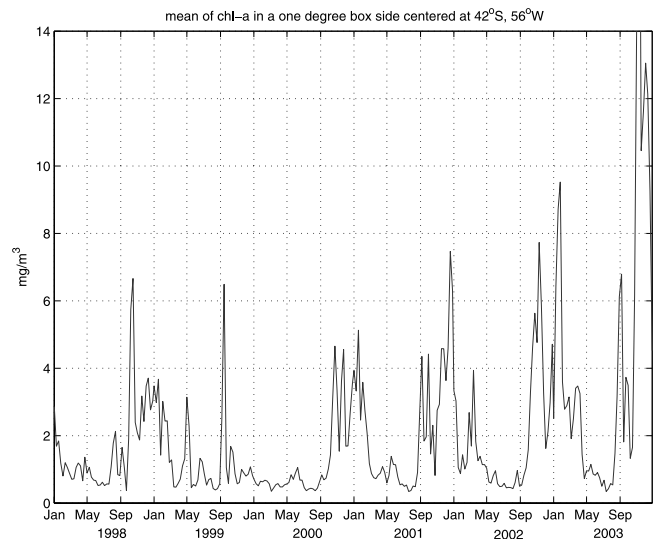


Figure 8. Chl *a* time series averaged on a 1° box side centered at 40.25°S , 56.73°W , i.e., in the northern part of the PSB region.

[35] An anticyclonic flow, with a mean barotropic transport higher than 100 Sv , has been estimated around the Zapiola Rise [*Saunders and King*, 1995]. Modeling studies suggest that the anticyclonic circulation is maintained by eddy-driven potential vorticity fluxes accelerating the flow within the closed potential vorticity contours that surround the rise [*de Miranda et al.*, 1999]. Using altimetry data, *Fu et al.* [2001] showed that at intraseasonal scales the closed

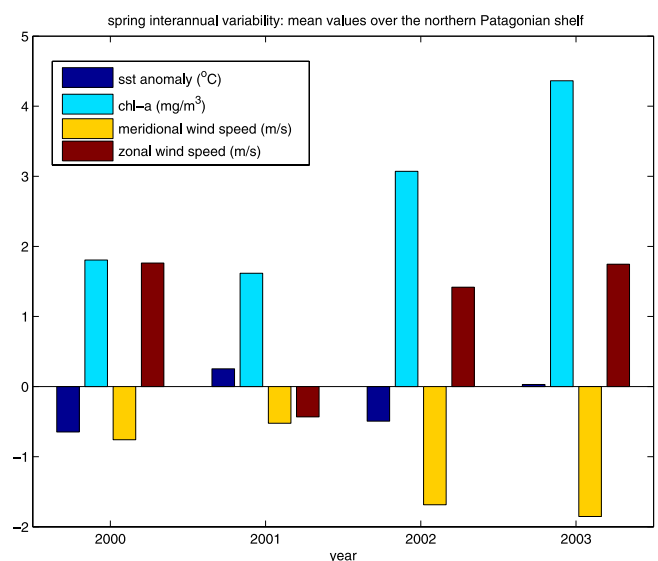


Figure 9. Spatial average on a 1° box side (centered at 40.25°S , 56.73°W) and time mean for austral spring (21 September to 21 December) of SST anomaly (dark blue), chl *a* (cyan), meridional wind speed (yellow), and zonal wind speed (brown) for the 4 years (2000–2003) where data are concomitant. SST data are from *Reynolds and Smith* [1994]. The SST anomaly is obtained as the difference between the raw data and the fit of a sinusoidal function (in the least square sense) to the data.

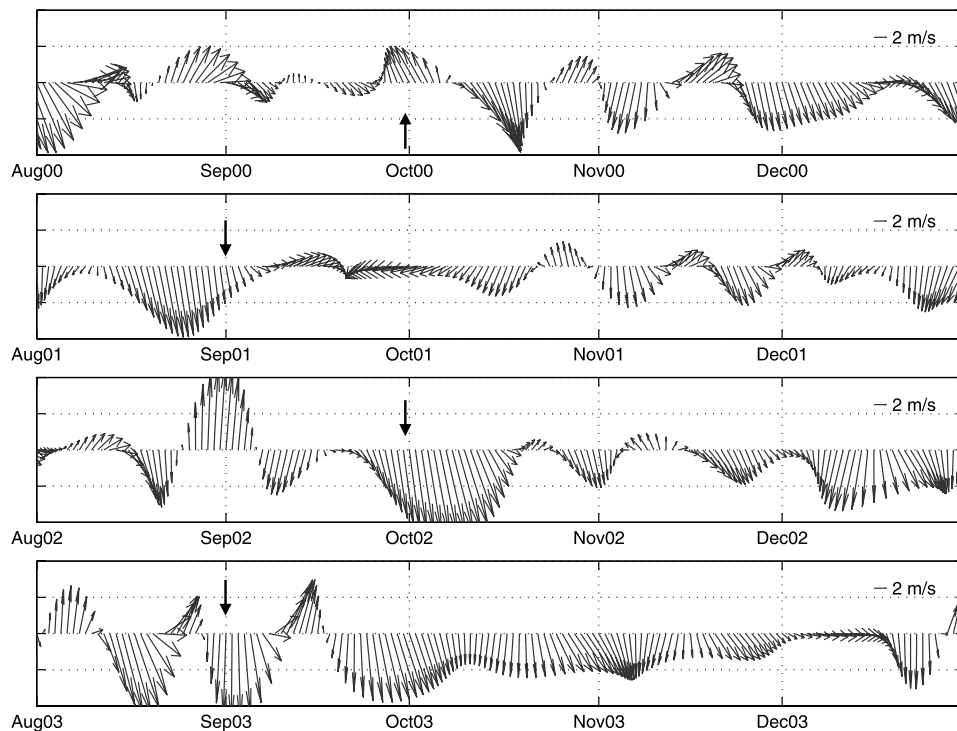


Figure 10. Time series of the QuickScat wind speed data averaged on a 1° box side centered at 40.25°S , 56.73°W . Only the August–December period of the 2000–2003 time series is shown. Data are low-pass filtered with a cutoff frequency of 15 days. Solid arrows indicate the beginning of the first strong spring chl *a* bloom of the year.

potential vorticity contours provide a mechanism for the confinement of topographic waves around the Zapiola Rise. These physical mechanisms may cause the dynamical isolation of the region, and therefore explain the local minimum in SST gradient and SLA, but do not explain why the bloom in the Zapiola Rise occurs in late summer and not in spring as in the surrounding areas (Figure 12). The monthly means of the mixed layer depth, as estimated by *Levitus and Boyer* [1994], do not present significant differences over the Zapiola Rise, with reference to the surroundings. Hence the stability of the water column does not seem to explain the lag between the Zapiola Rise and the surroundings. However, very few data are available in the region to build the monthly means of the mixed layer depth [*Levitus and Boyer*, 1994].

4.4. Brazil-Malvinas Collision front

[36] In the collision region (i.e., between 53.5 and 55°W and 37.5 and 40.5°S) the Malvinas and Brazil currents produce a very active front that is identified year-round in SST gradient and ocean color data. Following the along-shelf section shown in Figure 1, a time-coincident local maximum in chl *a* and SST gradient is observed within the northern and southern limits throughout the respective record lengths (Figures 13a and 13c). Similar along shore frontal displacements are present in chl *a* concentrations and SST gradients. Thus it is clear that the chl *a* concentration increases at the Brazil-Malvinas Collision front. The displacement of the front along the section is also observed between the same range of latitudes for the rest of the available chl *a* data (i.e., from January 1998, not shown)

and for the RSMAS SST gradient data set (i.e., from January 1985 to December 1995, not shown). The JPL data set shows excessive cloud masking in the region (see comments in section 2). In spite of the large interannual variability (both in position and magnitude) observed in chl *a* between 1998 and 2003, the front shows in general to shift northward in late winter and southward in late summer.

[37] The time average of chl *a* concentrations on the along-shelf section (Figure 13b) shows two local maxima, at 37 and 39.2°S , which respectively correspond to the northern and southern limits of the Brazil-Malvinas Collision front. Between these limits, the time average of the SST gradient values also presents the highest values of the section (Figure 13d). The time average of the SST section (Figure 13f) shows clearly that the transition region from the colder subantarctic waters (8°C) to the warmer Subtropical waters ($> 18^\circ\text{C}$) is contained between the limits previously defined. The inflection point of the curve in Figure 13f is located at 38.9°S , corresponding also to the latitude of the maximum in the SST gradient time average plot (Figure 13d). Thus we associate this point (54.2°W , 38.9°S) to the time-averaged position of the Brazil-Malvinas Collision front along the section. The intersection between the along-shelf section and the coincident mean positions of the SAF and BCF as estimated by *Saraceno et al.* [2004] is in good agreement (Figure 14) with the previous observation.

[38] South of 39.2°S , relatively high chl *a* values ($\sim 1.2 \text{ mg/m}^3$) are usually present from October to April (austral spring and summer). At that time, a strong bloom over the Patagonian Shelf Break is observed (see section 4.1),

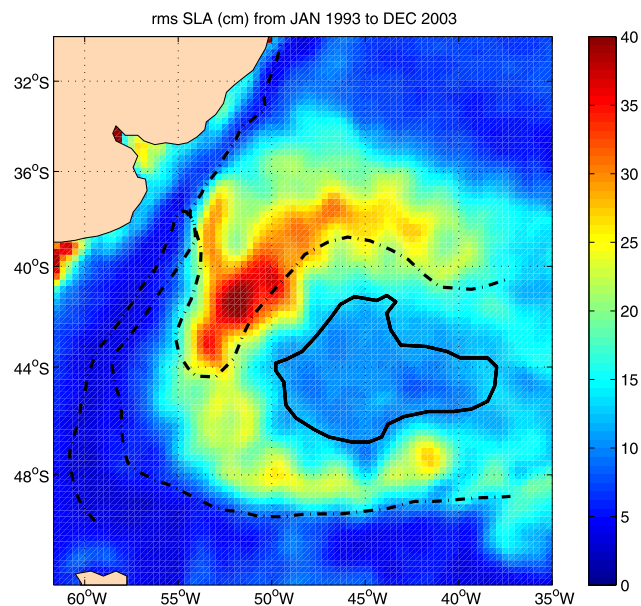


Figure 11. Root mean square of sea level anomaly (SLA) in cm from January 1993 to December 2003. Dash-dotted lines are mean positions of BCF and SAF (as in Figure 1). Solid black line is the contour of the Zapiola Rise region (as in Figure 3b). SLA maps were obtained from a complete reprocessing of TOPEX/Poseidon, ERS-1/2, and Jason data. Data are 7 days interpolated in time in a grid of $1/3^\circ$ of spatial resolution. The anomaly is calculated with regard to the mean of the first seven years. Altimeter products were produced by Ssalto/Duacs as part of the Environment and Climate EU Enact project (EVK2-CT2001-00117) and distributed by AVISO, with support from CNES.

which produces the high chl *a* concentration in the southern part of the section in Figure 13a.

[39] North of 37°S , subtropical waters present moderate values of chl *a* in austral winter. The intrusion of high nutrient subantarctic waters transported by eddies is probably responsible for these relatively high chl *a* values [L98;

Brandini *et al.*, 2000; Garcia *et al.*, 2004]. In particular, between September and November 2003, this observation is partly confirmed by the relatively low temperatures (Figure 13e) that are observed in the same regions where chl *a* is higher than normal (Figure 13a) north of 37°S .

[40] The time average of the SST gradient at the along-shelf section shows a range of about 200 km of maximum values between 37.6°S and 39°S (Figure 13d). This range of migration coincides with the separation between the summer and winter frontal positions derived from SST frontal probability maps obtained by Saraceno *et al.* [2004], which are schematically indicated in Figure 14. The range of migration of the chl *a* maximum along the section is of about 310 km (Figure 13b), exceeding by 55 km at each end of the SST gradient range of migration (Figure 14). The patchiness of the chlorophyll distribution is probably responsible of the larger alongshore range of migration of the chl *a* maximum with reference to the SST front. The mechanisms responsible for the observed motion of the surface expression of the BMF are not understood. In situ measurements show that the subsurface orientation of the front in summer is N-S [Provost *et al.*, 1996], matching the surface expression in austral winter. The relatively strong and shallow (<20 m) seasonal thermocline that develops in summer above the cold Malvinas Current may be responsible for the summer decoupling between the surface and subsurface temperature structures [Provost *et al.*, 1996; Saraceno *et al.*, 2004].

5. Summary and Discussion

[41] The upper layers in the western Argentine Basin present intense current systems, such as the BC and the MC, which are associated with strong thermohaline fronts. Cross frontal mixing creates small-scale thermohaline structures [Bianchi *et al.*, 1993, 2002], which may enhance the vertical stratification of subantarctic waters, and also lead to small-scale nutrient exchange [Brandini *et al.*, 2000]. In addition, current instabilities generate one of the most energetic eddy regions of the World Ocean [Chelton *et al.*, 1990]. Thus it appears that most of the physical ingredients believed to be

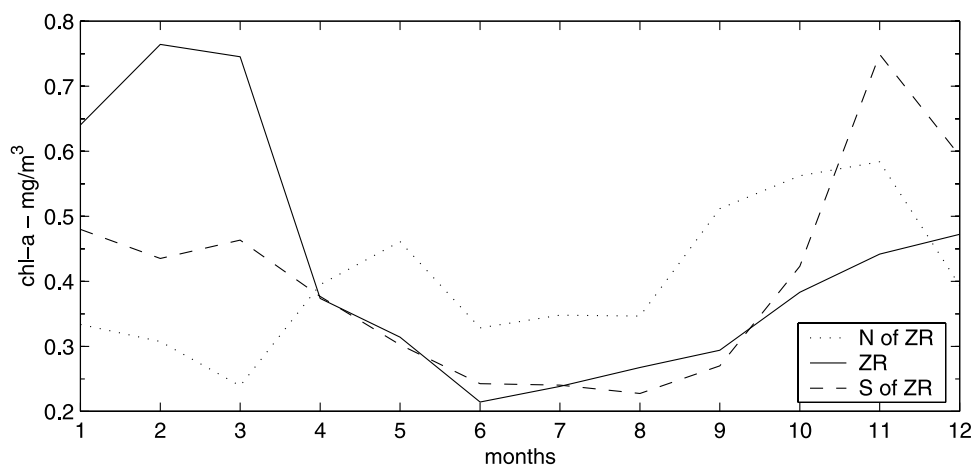


Figure 12. Chl *a* time series north (dotted line), south (dash-dotted line) and over (solid line) the Zapiola Rise. The precise location of the points where time series are extracted, is indicated on Figure 3b. Each value in the time series is the mean within a box of ~ 30 km per side in the monthly climatology.

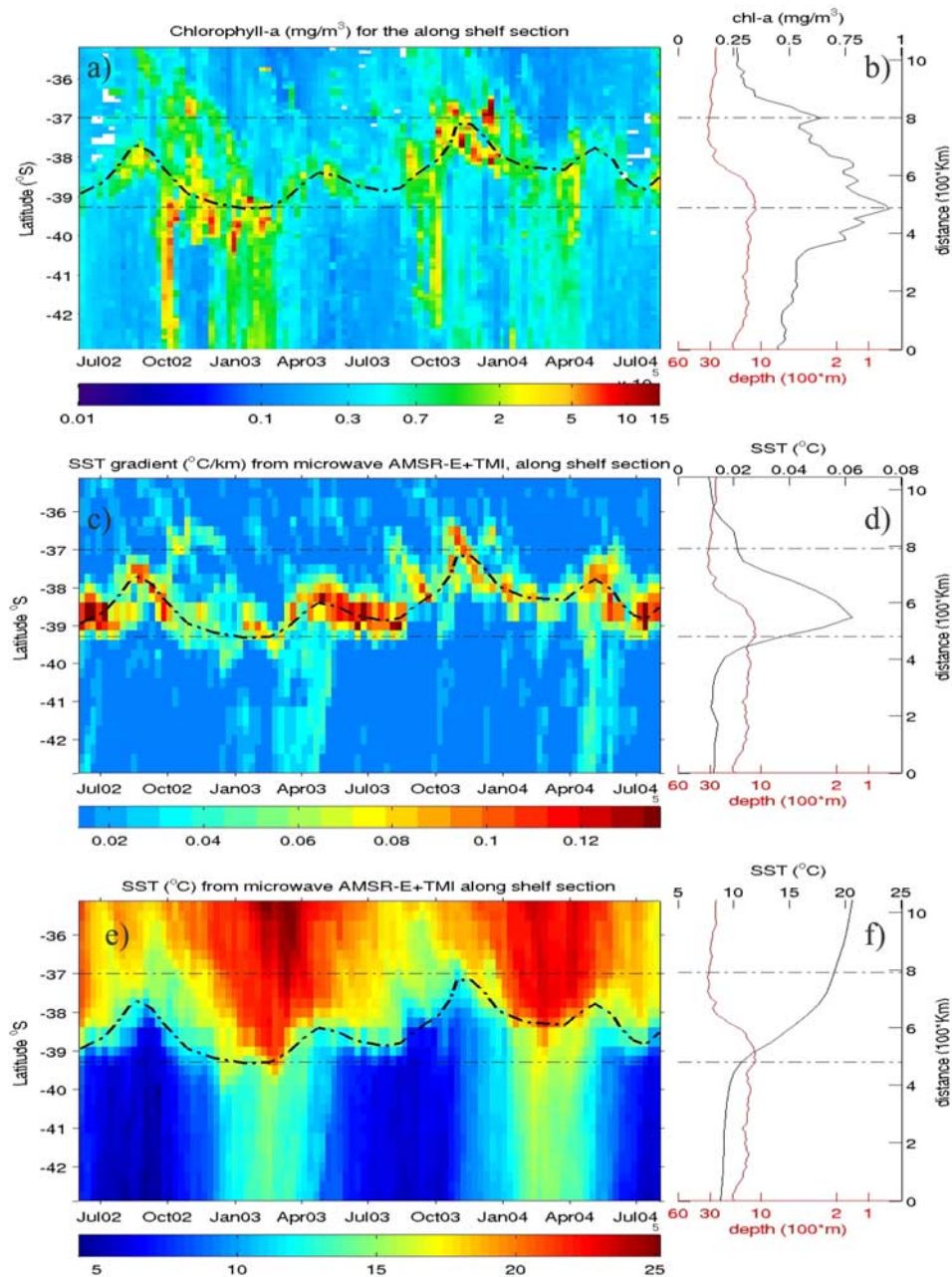


Figure 13. (a) Chl a (mg/m^3), (c) SST gradient ($^{\circ}\text{C/km}$), and (e) SST ($^{\circ}\text{C}$) versus time for the along-shelf section. The position of the section is indicated in Figure 1. The bathymetry and the time average of the (b) chl a , (d) SST gradient and (f) SST along the section are indicated in the plots to the right of the space-time figures. Chl a local maxima are indicated with dash-dotted lines and reported in the SST and SST gradient sections.

important in the development of chl a blooms are ubiquitous features of this part of the southwestern South Atlantic. The near coincidence between open ocean SST fronts and chl a maxima in the collision and overshoot regions suggests that frontal dynamics plays an important role in causing the observed blooms in these regions.

[42] The major results and observations from this study are as follows.

[43] 1. Using histogram analysis of mean SST, SST gradient and chl a images, we identified three new biogeographical regions with regard to L98 Provinces in the SWA:

the Patagonian Shelf Break, the Brazil Current Overshoot and the Zapiola Rise. These regions provide a more accurate description of the SWA.

[44] 2. Power spectral density of SST and chl a in the PSB region shows significant peaks at intraseasonal frequencies. Coastal-trapped waves are suggested as a possible mechanism leading to the variability observed.

[45] 3. Mesoscale activity associated with the BCF and in particular eddies drifting southward are probably responsible for the high chl a values observed throughout the Brazil Current Overshoot region.

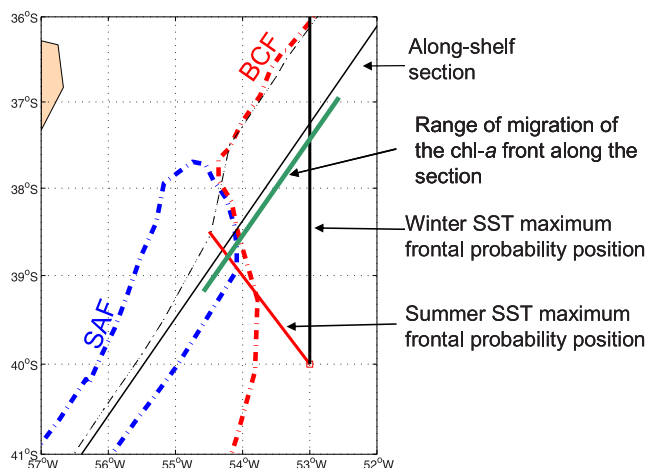


Figure 14. Schematic positions of the surface fronts in the BM collision region. Summer and winter frontal probability positions of the BCF and SAF are from *Saraceno et al.* [2004]. The dash-dotted line is the 1000 m isobath. The green segment is the range of migration of the chl *a* front along the along-shelf section (thin black line).

[46] 4. Chl *a* maximum in the Zapiola Rise region and in the southwestern part of the overshoot region is observed in February, three months later than in the surrounding waters. Mechanisms to explain the delay in the bloom in this region are still unknown. In situ data are necessary to describe the subsurface structure and understand the underlying processes.

[47] 5. Significant interannual variability in chl *a* over the Patagonian shelf break region is observed, especially in spring. Highest chl *a* concentrations seem associated with stronger local northerly wind speed that results in an eastward transport of shelf water to the nutrient-rich waters of the Malvinas Current. It is suggested that the resulting interleaving of water masses may enhance vertical stability and thus retains phytoplankton cells in the euphotic zone

[*Podestá*, 1990]. Further analyses and comparison with in situ data are necessary to assess these hypotheses.

[48] 6. The Brazil-Malvinas front is detected using both SST gradient and SeaWiFS images. The time-averaged position of the front at 54.2°W is estimated at 38.9°S and its alongshore migration of about 300 km. This result agrees with that of *Saraceno et al.* [2004]. To describe, and better understand the potential impact of the frontal movements on the chlorophyll fields, the analysis of consecutive instantaneous and coincident high-resolution SST, SST gradient, and chl *a* fields have been undertaken using Moderate-Resolution Imaging Spectroradiometer (MODIS) data [*Barre et al.*, 2005].

[49] The important interannual variability in the chl *a* fields observed in the two time-space sections and in the time series (respectively Figures 5, 13, and 8) lead us to estimate the interannual standard deviation (ISD, equation (1)) and compare it to the monthly standard deviation (MSD, equation (2)) in the SWA, defined as follows:

$$\text{ISD} = \sqrt{\frac{\sum_{ij} (\text{chl}(i,j) - \langle \text{chl}(i) \rangle_j)^2}{N-1}} \quad (1)$$

$$\text{MSD} = \sqrt{\frac{\sum_{ij} (\text{chl}(i,j) - \langle \text{chl} \rangle_{ij})^2}{N-1}} \quad (2)$$

where j spans the 6 years (1998–2003) of chl *a*, i spans the 12 months of the year, *chl* is a matrix containing the 72 (N) monthly means of chl *a* and the brackets indicate average over the index (thus $\langle \text{chl}(i) \rangle_j$ in A are the monthly climatologies of chl *a* and $\langle \text{chl} \rangle_{ij}$ in B is the mean field of chl *a*).

[50] The interannual and monthly standard deviation maps and their ratio (ISD/MSD) are presented in Figure 15. The ISD represents a high portion (higher than 0.7) of the MSD

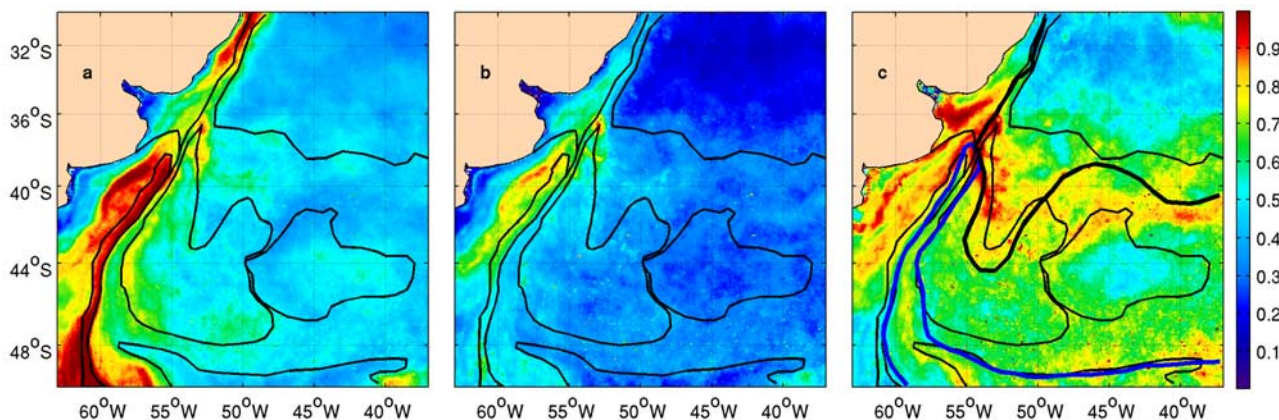


Figure 15. (a) Monthly chl *a* standard deviation, (b) interannual chl *a* standard deviation (see formula in the text), and (c) ratio of interannual and monthly standard deviation ($c = b/a$). Log of monthly means was considered because attenuate the contrast between the higher and lower values. Units in Figures 15a and 15b are $\log(\text{mg}/\text{m}^3)$. The three fields are scaled between 0 and 1. Thin black lines are contours of the biophysical regions defined in Figure 3. Thick lines in Figure 15c are the SAF (blue) and BCF (black), as described in Figure 1.

in the B/M Collision region and in general along the BCF (Figure 15c). From 36 to 40°S, the highest ratio values precisely follows the B/M Collision front (i.e., where the BCF and SAF coincide), indicating the important interannual variability of the chl *a* in that region. High ratio values are also present over the FKLD region north of 45°S. In contrast, the BRAZ region shows high ratio values only at the mouth of La Plata River. SATL and Zapiola Rise regions also show low interannual variability. The PSB and overshoot regions show intermediate ratio values, while higher ratio values are present over the MC.

[51] The results presented here include a wide range of different phenomena. Most of the results are descriptions of simple calculations that raise an important number of unresolved issues in the region, e.g., (1) the important interannual chl *a* variability in almost the whole SWA, (2) the mechanism driving the chl *a* distribution over the Zapiola Rise, (3) the variability of the boundaries of the biophysical regions. As longer time series of satellite data become available, a more accurate description of the interannual variability will be possible. However, satellite data alone are not sufficient to measure many aspects of the relationship between fronts and chl *a*. Analyses of satellite and in situ data combined with modeling studies should be undertaken to improve our understanding of phytoplankton bloom dynamics in the SWA.

[52] **Acknowledgments.** The Goddard Space Flight Center (GSFC/NASA) provided the SeaWiFS data used in this work. AVHRR data described as from RSMAS were collected by Servicio Meteorológico Nacional, Fuerza Aérea Argentina, as part of a cooperative study of that organization with the University of Miami. V. Garçon provided many useful comments on an earlier version of the manuscript. Discussions with Y. Dandonneau about chl *a* distribution on the Zapiola-Rise are duly acknowledged. M.S. is supported by a fellowship from Consejo Nacional de Investigaciones Científicas y Técnicas (Argentina). A.R.P. was supported by grant CRN-61 from the Inter-American Institute for Global Change Research and PICT99 07-06420 from Agencia Nacional de Promoción Científica y Tecnológica, Argentina. Constant support from CNES (Centre National d'Études Spatiales) is acknowledged.

References

- Acha, E. M., H. W. Mianzan, R. A. Guerrero, M. Favero, and J. Bava (2004), Marine fronts at the continental shelves of austral South America—Physical and ecological processes, *J. Mar. Syst.*, *44*, 83–105.
- Barre, N., C. Provost, and M. Saraceno (2005), Spatial and temporal scales of the Brazil-Malvinas Confluence region documented by MODIS high resolution simultaneous SST and color images, *Adv. Space Res.*, in press.
- Bianchi, A. A., C. F. Giulivi, and A. R. Piola (1993), Mixing in the Brazil/Malvinas Confluence, *Deep Sea Res.*, *40*, 1345–1358.
- Bianchi, A. A., A. R. Piola, and G. Collino (2002), Evidence of double-diffusion in the Brazil/Malvinas Confluence, *Deep Sea Res., Part I*, *49*, 41–52.
- Bianchi, A. A., L. Biancucci, A. R. Piola, D. Ruiz Pino, I. Schloss, A. R. Poisson, and C. F. Balestrini (2005), Vertical stratification and air-sea CO₂ fluxes in the Patagonian shelf, *J. Geophys. Res.*, C07003, doi:10.1029/2004JC002488.
- Bisbal, G. (1995), The southeast South American shelf large marine ecosystem: Evolution and components, *Mar. Policy*, *19*, 21–38.
- Brandini, F. P., D. Boltovskoy, A. Piola, S. Kocmur, R. Rottgers, P. Cesar Abreu, and R. Mendes Lopes (2000), Multiannual trends in fronts and distribution of nutrients and chlorophyll in the southwestern Atlantic (30–62°S), *Deep Sea Res., Part I*, *47*, 1015–1033.
- Chelton, D. B., M. G. Schlax, D. L. Witter, and J. G. Richman (1990), GEOSAT altimeter observations of the surface circulation of the Southern Ocean, *J. Geophys. Res.*, *95*, 17,877–17,903.
- Dandonneau, Y., P.-Y. Deschamps, J.-M. Nicolas, H. Loisel, J. Blanchot, Y. Montel, F. Thieuleux, and G. Becu (2004), Seasonal and interannual variability of ocean color and composition of phytoplankton communities in the North Atlantic, equatorial Pacific and South Pacific, *Deep Sea Res., Part II*, *51*, 303–318.
- de Miranda, A. P., B. Barnier, and W. Dewar (1999), On the dynamics of the Zapiola Anticyclone, *J. Geophys. Res.*, *104*, 21,137–21,149.
- Erickson, D. J., III, J. L. Hernandez, P. Ginoux, W. W. Gregg, C. McClain, and J. Christian (2003), Atmospheric iron delivery and surface ocean biological activity in the Southern Ocean and Patagonian region, *Geophys. Res. Lett.*, *30*(12), 1609, doi:10.1029/2003GL017241.
- Escoffier, C., and C. Provost (1998), Surface forcing over the southwest Atlantic from NCEP and ECMWF reanalyses on the period 1979–1990, *Phys. Chem. Earth*, *23*, 7–8.
- Food and Agricultural Organization (FAO) (1972), *Atlas of the Living Resources of the Sea*, Rome.
- Framiñan, M. B., and O. B. Brown (1996), Study of the Río de la Plata turbidity front. Part I: Spatial and temporal distribution, *Cont. Shelf Res.*, *16*(10), 1259–1282.
- Fratantoni, D. M., and D. A. Glickson (2002), North Brazil Current ring generation and evolution observed with SeaWiFS, *J. Phys. Oceanogr.*, *32*(3), 1058–1074.
- Fu, L.-L., B. Cheng, and B. Qiu (2001), 25-day period large-scale oscillations in the Argentine Basin revealed by the TOPEX/Poseidon altimeter, *J. Phys. Oceanogr.*, *31*(2), 506–517.
- García, C. A. E., Y. V. B. Sarma, M. M. Mata, and V. M. T. Garcia (2004), Chlorophyll variability and eddies in the Brazil-Malvinas Confluence region, *Deep Sea Res., Part II*, *51*, 159–172.
- Garçon, V. C., A. Oschlies, S. C. Doney, D. McGillicuddy, and J. Waniek (2001), The role of mesoscale variability on plankton dynamics in the North Atlantic, *Deep Sea Res., Part II*, *48*, 2199–2226.
- Ghil, M., et al. (2002), Advanced spectral methods for climatic time series, *Rev. Geophys.*, *40*(1), 1003, doi:10.1029/2000RG000092.
- Goni, G. J., and I. Wainer (2001), Investigation of the Brazil Current front variability from altimeter data, *J. Geophys. Res.*, *106*, 31,117–31,128.
- Gordon, A. L. (1981), South Atlantic thermocline ventilation, *Deep Sea Res., Part A*, *28*, 1239–1264.
- Gordon, A. L., and C. L. Greengrove (1986), Geostrophic circulation of the Brazil-Falkland Confluence, *Deep Sea Res., Part A*, 573–585.
- Gregg, W. W., N. W. Casey, and C. R. McClain (2005), Recent trends in global ocean chlorophyll, *Geophys. Res. Lett.*, *32*, L03606, doi:10.1029/2004GL021808.
- Hormazabal, S., G. Shaffer, J. Letelier, and O. Ulloa (2001), Local and remote forcing of sea surface temperature in the coastal upwelling system off Chile, *J. Geophys. Res.*, *106*, 16,657–16,672.
- Huthnance, J. M. (1995), Circulation, exchange and water masses at the ocean margin: The role of physical processes at the shelf edge, *Prog. Oceanogr.*, *35*(4), 353–431.
- Legeckis, R., and A. L. Gordon (1982), Satellite-observations of the Brazil and Falkland Currents—1975 to 1976 and 1978, *Deep Sea Res., Part A*, *29*, 375–401.
- Lentini, C. A. D., D. B. Olson, and G. P. Podesta (2002), Statistics of Brazil Current rings observed from AVHRR: 1993 to 1998, *Geophys. Res. Lett.*, *29*(16), 1811, doi:10.1029/2002GL015221.
- Levitus, S., and T. Boyer (1994), *World Ocean Atlas 1994*, vol. 4, *Temperature*, NOAA Atlas NESDIS 4, NOAA, Silver Spring, Md.
- Longhurst, A. (1998), *Ecological Geography of the Sea*, Elsevier, New York.
- Martos, P., and M. C. Piccolo (1988), Hydrography of the Argentine continental shelf between 38° and 42°S, *Cont. Shelf Res.*, *8*(9), 1043–1056.
- McClain, C. R., M. L. Cleave, G. C. Feldman, W. W. Gregg, S. B. Hooker, and N. Kuring (1998), Science quality SeaWiFS data for global biosphere research, *Sea Technol.*, *39*(9), 10–16.
- McGillicuddy, D. J., Jr., A. R. Robinson, D. A. Siegel, H. W. Jannasch, R. Johnson, T. D. Dickey, J. McNeil, A. F. Michaels, and A. H. Knap (1998), Influence of mesoscale eddies on new production in the Sargasso Sea, *Nature*, *394*, 263–266.
- Olson, D. B., G. P. Podesta, R. H. Evans, and O. B. Brown (1988), Temporal variations in the separation of Brazil and Malvinas Currents, *Deep Sea Res., Part A*, *35*, 1971–1990.
- Peterson, R. G., and L. Stramma (1991), Upper-level circulation in the South Atlantic Ocean, *Prog. Oceanogr.*, *26*(1), 1–73.
- Piola, A. R., and A. L. Gordon (1989), Intermediate waters of the western South Atlantic, *Deep Sea Res.*, *36*, 1–16.
- Podestá, G. P. (1990), Migratory pattern of Argentine hake *Merluccius hubbsi* and oceanic processes in the southwestern Atlantic Ocean, *Fish. Bull.*, *88*(1), 167–177.
- Podestá, G. P., O. B. Brown, and R. H. Evans (1991), The annual cycle of satellite-derived sea surface temperature in the southwestern Atlantic Ocean, *J. Clim.*, *4*, 457–467.
- Provost, C., O. Garcia, and V. Garçon (1992), Analysis of satellite sea surface temperature time series in the Brazil-Malvinas Current confluence region: Dominance of the annual and semiannual periods, *J. Geophys. Res.*, *97*, 17,841–17,858.

- Provost, C., V. Garçon, and L. M. Falcon (1996), Hydrographic conditions in the surface layers over the slope-open ocean transition area near the Brazil-Malvinas confluence during austral summer 1990, *Cont. Shelf Res.*, *16*(2), 215–219.
- Quartly, G. D., and M. A. Srokosz (2003), A plankton guide to ocean physics: Colouring in the currents round South Africa and Madagascar, *Ocean Challenge*, *12*(3), 19–23.
- Reynolds, R. W., and T. M. Smith (1994), Improved global sea surface temperature analyses using optimum interpolation, *J. Clim.*, *7*, 929–948.
- Roden, G. I. (1986), Thermohaline fronts and baroclinic flow in the argentine basin during the austral spring of 1984, *J. Geophys. Res.*, *91*, 5075–5093.
- Russ, J. C. (2002), *The Image Processing Handbook*, CRC Press, Boca Raton, Fla.
- Saraceno, M., C. Provost, A. R. Piola, J. Bava, and A. Gagliardini (2004), Brazil Malvinas Frontal System as seen from 9 years of advanced very high resolution radiometer data, *J. Geophys. Res.*, *109*, C05027, doi:10.1029/2003JC002127.
- Saunders, P. M., and B. A. King (1995), Bottom currents derived from a shipborne ADCP on WOCE cruise A11 in the South Atlantic, *J. Phys. Oceanogr.*, *25*(3), 329–347.
- Smith, W. H. F., and D. T. Sandwell (1994), Bathymetric prediction from dense satellite altimetry and sparse shipboard bathymetry, *J. Geophys. Res.*, *99*, 21,803–21,824.
- Vazquez, J., K. Perry, and K. Kilpatrick (1998), NOAA/NASA AVHRR Oceans Pathfinder sea surface temperature data set user's reference manual version 4.0, *JPL Publ.*, *D-14070*.
- Vivier, F., and C. Provost (1999), Direct velocity measurements in the Malvinas Current, *J. Geophys. Res.*, *104*, 21,083–21,104.
- Vivier, F., C. Provost, and M. P. Meredith (2001), Remote and Local Forcing in the Brazil-Malvinas Region, *J. Phys. Oceanogr.*, *31*(4), 892–913.
- Wentz, F., and T. Meissner (2004), AMSR-E/Aqua Daily L3 Global Ascending/Descending.25 x.25 deg Ocean Grids V001, June 2002 to December 2003, http://nsidc.org/data/ae_dyocn.html, Natl. Snow and Ice Data Cent., Boulder, Colo. (Updated daily.)

A. R. Piola, Departamento de Oceanografía, Servicio de Hidrografía Naval, Avenida Montes de Oca 2124, 1271 Buenos Aires, Argentina.

C. Provost and M. Saraceno, LODYC, UMR 7617 CNRS, IRD-UPMC-MNHN, Institut Pierre Simon Laplace, Université Pierre et Marie Curie, Tour 45, Etage 5, Boite 100, 4 Place Jussieu, F-75252 Paris Cedex 05, France. (martin.saraceno@lodyc.jussieu.fr)